Journal of Geoscience and Environment Protection, 2019, 7, 251-267
http://www.scirp.org/journal/gep
ISSN Online: 2327-4344
ISSN Print: 2327-4336

A Multiscale Energetic Diagnosis of the Response of Mokpo Sea to Typhoon Bolaven

Xia Chai[1,2], Lin Wang[3]

[1]School of Marine Sciences, Nanjing University of Information Science and Technology, Nanjing, China
[2]China Meteorological Press, Beijing, China
[3]Marine Monitoring and Forecasting Center of Zhejiang Province, Hangzhou, China
Email: chaixia.v@qq.com

How to cite this paper: Chai, X., & Wang, L. (2019). A Multiscale Energetic Diagnosis of the Response of Mokpo Sea to Typhoon Bolaven. *Journal of Geoscience and Environment Protection, 7,* 251-267.
https://doi.org/10.4236/gep.2019.78019

Received: May 17, 2019
Accepted: August 24, 2019
Published: August 27, 2019

Abstract

The ocean response to typhoon is usually characterized by a cooling on the sea surface. In August 2012, however, a warming (instead of cooling) event occurs in the Yellow Sea outside Mokpo, South Korea, as the typhoon Bolaven (2012) passes. This study gives a brief introduction to this abnormal sea surface warming. It also provides a multiscale energetic diagnosis of the oceanic response to Typhoon Bolaven. We used a recently developed analysis tool named "multiscale window transform" (MWT). Based on the MWT, we also expanded a localized multiscale energy and vorticity analysis (MS-EVA). The fields are reconstructed onto three scale windows: large-scale, abnormal warming-scale, and high frequency tide-scale windows. The results show that the kinetic energy (KE) in the abnormal warming-scale window of the Mokpo area is obviously enhanced during the passage of Bolaven, which can be attributed to three processes: transfer, transport process of KE and wind stress work. At the same time, the large-scale window in the Mokpo area experiences barotropic instabilities with KE transfers from large-scale window to warming-scale window. Besides, the strong wind stress bought by the passage of Bolaven not only inputs a large amount of KE into warming-scale window, but also causes the increase of KE flux convergence.

Keywords

Typhoon, Yellow Sea, Ocean Response, Air-Sea Interaction, Energetic Diagnose

1. Introduction

Tropical cyclone, which is also known as typhoon in the Pacific, is one of the most devastating storm systems that involves strong air-sea interactions. The

passage of typhoon is usually accompanied with numerous energy injection into the ocean (Chen et al., 2013; D'Asaro et al., 2013; Zhang et al., 2016; He et al., 2018; Han et al., 2017; Cheng et al., 2013), which will unavoidably alter the seawater column structure (Li et al., 2012; Price, 1981), sediment transport and deposition (Chang et al., 2001), and marine biochemical processes (Huang et al., 2011). Among these, the most prominent response is the cooling of sea surface temperature (SST) in the open ocean. In general, the SST drop induced by typhoon can exceed 3˚C, and even up to 7˚C - 11˚C in some cases. It is agreed that the cooling primarily results from typhoon-induced turbulence mixing and vertical entrainment of deep waters up to the ocean mixed layer (Chang et al., 2010; Liu et al., 2014; Moon et al., 2012; Lee et al., 2017; Lin et al., 2008; Price, 1981).

Due to the unique and complex geographical environment, East Asia has always experienced frequent natural disasters. Among them, typhoon disasters have attracted much attention because of their high frequency, heavy damage, a wide range of influence and long chain of disasters. In recent years, the rapid growth of population and economy in coastal areas has made these areas likely to suffer more significant losses in the face of typhoon attacks. Under such circumstances, a comprehensive and in-depth study of the typhoon has become a major issue related to the national economy and the people's livelihood. On the other hand, it is also important and urgent to analyze the possible trends in tropical cyclone activity in the context of global climate change. However, the ocean response to typhoon passage does not always manifest as SST drop, especially in the coastal area. Recently, Xie et al. (2017) reported that the typhoon-caused local SST change east to Hainan Island actually can be put into three types: warmed SST, slightly changed SST and cooled SST; the warmed SST is formed as a nonlinear soliton excited by the typhoon transports heat northward toward the coastal area. Another example is in Daya Bay (Li & Xu, 1994), where the bulk water temperature may be increased after typhoons move westward across the South China Sea. Li & Xu (1994) found that the adjustment of vertical circulation may contribute to the destratification of the water column, and hence lead to the rising of water temperature. The same warming event near Jiangsu coast was also reported (Yang et al., 2017), but with little attention.

This paper is based on Typhoon Bolaven occurred in 2012, and thus this can be mainly a case study. Bolaven formed as a tropical depression over the western Pacific Ocean on August 20, 2012, and strengthened to a typhoon the following day. At around 15:15 on the 28th, it landed on the coast of southwestern Korea. It caused large-scale heavy rainfall and windy weather in northeastern China, North Korea, and South Korea. We will report another abnormal SST rise after typhoon passage. This warming event is special in that it is related to the specific hydrographic feature of the Yellow Sea, the Yellow Sea Surface Cold Patch (SCP) outside Mokpo. This study focuses on the dynamic process of the sea surface in addition to changes of SST during the passage of typhoon. In the following, we first introduce the typhoon, which we will be investigating, and its track (Section

2). Section 3 gives a brief introduction to the new methodology. Then we describe the ocean response based on observation and numerical simulation (Section 4). In Section 5 a detailed diagnosis of the multiscale dynamic based on the model result is provided. This study is summarized in Section 5.2.

2. Typhoon Track

The warming event we will be reporting occurs in August 2012 as the typhoon Bolaven (2012) passes the Yellow Sea. We need the best track of it, which is made available by the China Meteorological Administration (CMA) at www.tcdata.typhoon.org.cn. As shown in Figure 2, on 20 August 2012, Bolaven (2012) develops as a tropical depression in the western North Pacific, then intensifies and moves northwestward. It reaches the East China Sea and begins to weaken on 26 August. As of 28 August, Bolaven (2012) depresses as a tropical storm near the region west of Korean Peninsula and makes landfall. During 27 to 28 August, Bolaven (2012) passes the region off Mokpo, South Korea. The SST in this area has since experienced an abnormal rise during this period (see Figure 1).

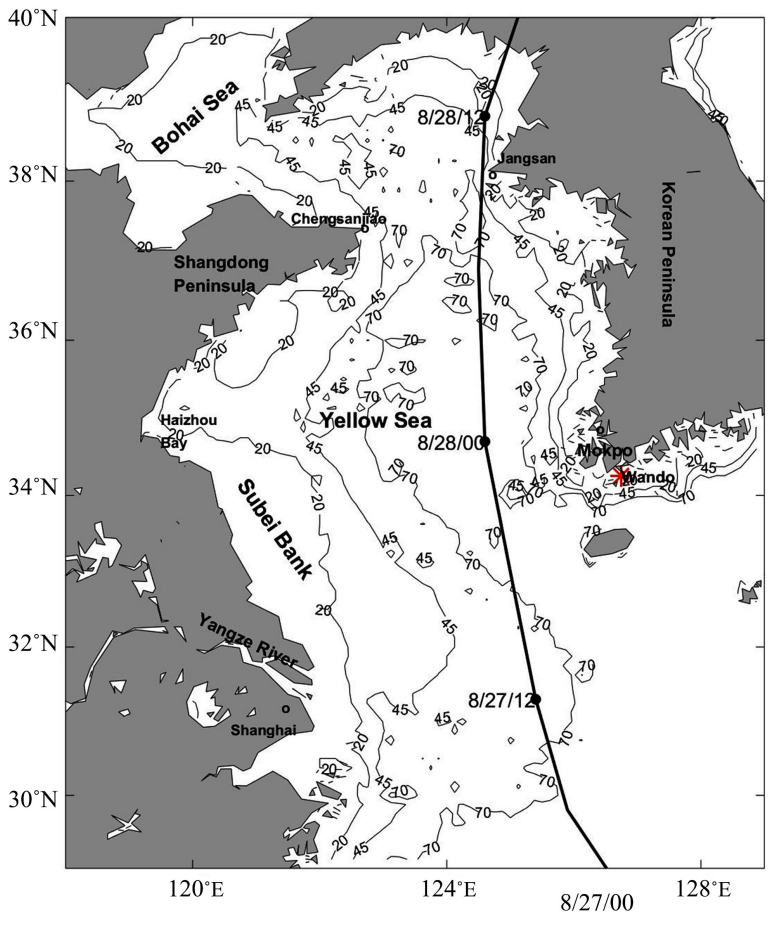

Figure 1. Best track of typhoon Bolaven (2012) (thick line) with date information (Courtesy of CMA). The time is Local Time. Black contours represent the topography of the Yellow Sea and the Bohai Sea. Unit for the contours: meter.

3. Energy Analysis Tool

The new methodology to be used in this research is the localized Multiscale Energy and Vorticity Analysis (MS-EVA) developed by Liang (2016), which is based on a new functional analysis tool, namely, the multiscale window transform (MWT) (Liang & Robinson, 2007). With the MWT, the function space can be split into a direct sum of several mutually orthogonal subspaces, each with an exclusive range of time scales, while having its local properties preserved (Wang & Liang, 2017).

In this study, we will use the MWT to decompose the original fields into two orthogonal windows, i.e., the mean flow window with low frequency and the eddy window with high frequency. For convenience, they are denoted by $\varpi = 0.1$, respectively. The kinetic energy (KE) and the available potential energy (APE) on the window ϖ are represented as

$$K^{\varpi} = \frac{1}{2}\rho_0 \hat{u}_H^{\sim\varpi} \cdot \hat{u}_H^{\sim\varpi}, \text{ and} \tag{1}$$

$$A^{\varpi} = \frac{g^2}{2\rho_0 N^2}\left(\hat{\rho}^{\sim\varpi}\right)^2 \tag{2}$$

where g is the gravity acceleration, ρ_0 is the reference density, ρ is the density perturbation from the background profile $\bar{\rho}(z)$, $N = \sqrt{-g\left(\partial\bar{\rho}/\partial z\right)/\rho_0}$ is the buoyance frequency, $u_H = (u, v)$ is the horizontal velocity vector and $(\cdot)$ is the MWT on window ϖ. Liang (2016) has given a detailed derivation of K^{ϖ} and A^{ϖ} equations. As in this study, we use the summarized results as follows:

$$\begin{aligned}
&\frac{\partial K^{\varpi}}{\partial t} + \overbrace{\nabla\cdot\left[\frac{1}{2}\rho_0 \hat{u}^{\sim\varpi}\left(\overbrace{uu_H}^{\sim\varpi}\right)\right]}^{\nabla\cdot Q_K^{\varpi}} \\
&= \overbrace{\nabla\cdot\left[\hat{u}^{\sim\varpi}\hat{p}^{\sim\varpi}\right]}^{\nabla\cdot Q_P^{\varpi}} - \underbrace{\left[\frac{1}{2}\rho_0\left(\hat{u}^{\sim\varpi}\right)^2\nabla\cdot u_u^{\varpi} + \frac{1}{2}\rho_0\left(\hat{v}^{\sim\varpi}\right)^2\nabla\cdot u_v^{\varpi}\right]}_{\Gamma_K^{\varpi}} \\
&\quad + \underbrace{\left(-g\hat{\rho}^{\sim\varpi}\hat{w}^{\sim\varpi}\right)}_{b^{\varpi}} + F_K^{\varpi}
\end{aligned} \tag{3}$$

$$\underbrace{\frac{\partial A^{\varpi}}{\partial t} + \nabla\cdot\left[\frac{g^2}{2\rho_0 N^2}\hat{\rho}^{\sim\varpi}\left(\overbrace{\rho u}^{\varpi}\right)\right]}_{\nabla\cdot Q_A^{\varpi}} = \underbrace{-A^{\varpi}\nabla\cdot u_{\rho}^{\varpi}}_{\Gamma_A^{\varpi}} + \underbrace{g\hat{\rho}^{\sim\varpi}\hat{w}^{\sim\varpi}}_{-b^{\varpi}} + F_A^{\varpi} \tag{4}$$

where p is the dynamic pressure and $u = (u, v, w)$ is the three-dimensional velocity vector.

The Γ^{ϖ} terms in (3) and (4) indicate the local energy transfer in window ϖ, and is called the canonical transfer (Liang, 2016). The superscript $0 \to 1$ can be used to signify the energy transfer from the mean flow window ($\varpi = 0$) to the eddy window ($\varpi = 1$). For instance, the canonical KE (APE) transfer to eddy window ($\varpi = 1$) from mean flow window ($\varpi = 0$) is signified as $\Gamma_K^{0\to 1}$

($\Gamma_A^{0\to 1}$). These two transfer processes will correspond to the two important geophysical flow processes, the baroclinic instability and the barotropic instability (Liang & Robbinson, 2007). A positive $\Gamma_K^{0\to 1}$ ($\Gamma_A^{0\to 1}$) denotes KE or APEtransfers from the mean flow to the eddies via barotropic (baroclinic) instability. For a detailed introduction of the localized MS-EVA and the MS-EVA-based theory of finite-amplitude baroclinic and barotropic instability, the interested reader can refer to Liang (2016).

The rest terms in (3) and (4), i.e., the $\nabla\cdot Q^{\varpi}$ terms denote the nonlocal process of energy flux divergence through advection or pressure work; The b^{ϖ} term is the rate of buoyancy conversion connecting APE and KE. The F terms indicate the external forcing and internal dissipation processes.

4. The Warming Event off Mokpo

On the track of Bolaven (2012), there happens to be a hydrographic station, i.e., the Wando Station (**Figure 1**) operated by the National Fisheries Research and Development Institute, which is working and provides a time series of temperature from 25 August through 8 September. The data are available from Korean Oceanographic Data Center (KODC). As shown in **Figure 2** (the red line), the SST off Mokpo begins to increase from 25 August, reaching its maximum on 27 August, and then gradually falls back until 6 September. Obviously there is a significant sudden warming event in this region.

In order to see the details of the event, we appeal to the output of a well-validated model for the Yellow Sea, i.e., the "Estuarine, Coastal and Ocean Model" (ECOM-si), which covers the entire East China Sea, Yellow Sea and Bohai Sea, and some parts of the Pacific Ocean and the Japan Sea (Wu et al., 2014). Horizontally the model resolution varies from hundred meters to 2 - 3 kilometers; vertically it has twenty sigma layers, with refined resolution for upper layers. Besides, tides are included, and there is a wet/dry scheme for inter-tidal flats. Hence it is adequate for the purpose of this study. An in-depth description of the model, including its configuration, boundary conditions, turbulence closure schemes, special techniques, etc., is beyond the scope of this study; the reader is referred to Wu et al. (2011, 2014) for details.

We will use the hourly outputs for the period of Bolaven (2012) passage. We then first compare the SST at Wando Station to the KDOC data. The two are plotted together in **Figure 2**. As can be seen, the hourly model output shows almost the same warming trend as the daily observation during the period. Obviously, the two agree very well; the model is henceforth validated for the purpose of this study. Validations in other regions for other fields can be found in Wu et al. (2011, 2014) and Huang et al. (2017).

With the model output we are now able to see the spatial structure of the warming. **Figure 3** displays the simulated SST increase from 25 August to 29 August, the two days immediately before and after Bolaven (2012)'s passage (cf. **Figure 1**). In sharp contrast to the overall cooling induced by this typhoon (area

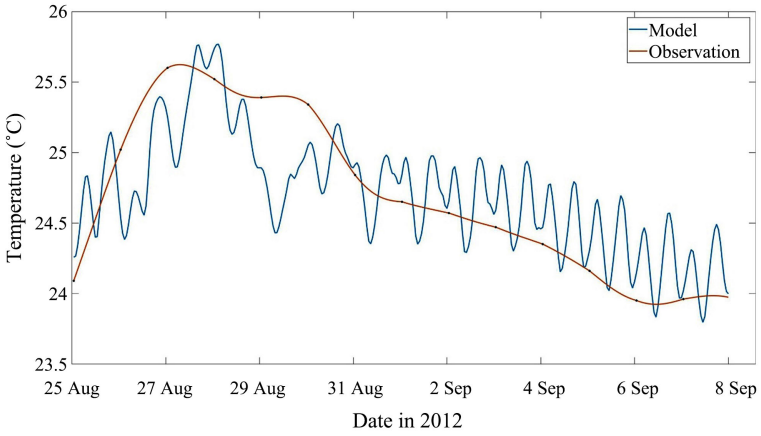

Figure 2. SST at the Wando station from the daily KODC data (red) and hourly model output (blue).

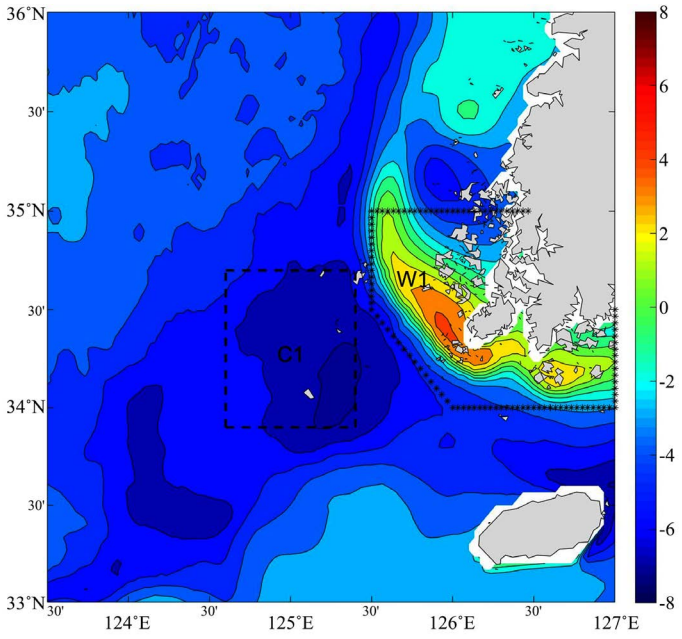

Figure 3. SST increase from 25 August to 29 August. W1 marks the warming area (Mokpo sea area), C1 indicates the cooling area.

C1), which has been reported elsewhere by Chang et al. (2014) and Liu et al. (2014), there is a significant warming signal off the southwestern tip of Korean Peninsula. The warming area is centered at a point off Mokpo, with a north-west-southeast extension of 100 - 200 km (W1 area).

5. Dynamic Analysis of Response in Mokpo Sea Area to Bolaven

Multi-scale energy analysis can be used to explore complex nonlinear dynamic processes in the ocean or atmosphere and interactions between different scales. For the warming phenomenon of about 1 week, the tide (the M2 partial tide dominated by the half-day period in the Yellow Sea region) does not contribute

to the scale. However, for other dynamic processes of the ocean under the typhoon, the contribution of this scale and its multi-scale interactions deserves further investigation.

5.1. Results of MWT

Using the Multi-scale Window Transform **(MWT)**, we reconstruct variations **(e.g., temperature)** from the model input into three scale window, namely large-scale ($\bar{\omega}=2$), abnormal warming-scale ($\bar{\omega}=1$), and high frequency tide-scale windows ($\bar{\omega}=0$). The parameters for MWT and MS-EVA are summarized in Table 1.

Figure 4(a) shows the time series of the SST field and its reconstructed fields (Figures 4(b)-(d)) in the Mokpo area. The selected time period is from August 15 to September 14, 2012, including the passage of the typhoon Bolaven (grey area in Figure 4). We can see that the original temperature field has an SST rise during the passage of typhoon, with the amplitude of 4˚C - 5˚C (Figure 4(a)). The temperature trend in the large-scale window changes little in the short term, with a slight cooling trend, and the amplitude is about 0.5˚C (Figure 4(b)). In the high-frequency tide-scale window, SST oscillates between −1˚C and 1˚C (Figure 4(d)). The main warming signal of the original field appears in the warming-scale window, with about 4˚C rise, which is consistent with the signal of the original field.

In general, the window boundary we selected here can separate the tidal signal, the background flow signal and the warming signal in the original sequence. It should be noted that the minimum-scale window we choose also contains other certain high-frequency signals such as inertial motion and internal waves, but the tidal signal is dominant, so the minimum-scale window can be called the high-frequency tide-scale window.

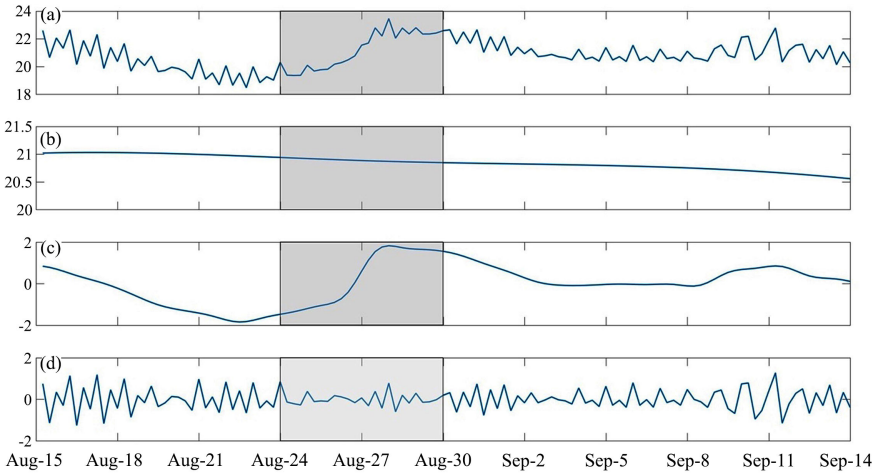

Figure 4. The original temperature field of area W1 (a) and its reconstruction on the large-scale window (b), warming-scale window (c) and high frequency tide-scale window (d) from 15 August to 14 September, 2012 (Units: ˚C). Grey area indicates the moments of Bolaven passing.

Table 1. The parameters for MWT and MS-EVA.

Parameter	Value
Period	2012.1.2.00-2013.5.27.18
Window bounds (j0, j1, j2)	5, 9, 11
Range	(119˚-127˚E, 31˚-37.2˚N)
Horizontal grid	241 × 187
Vertical levels	21

5.2. Multiscale Energy Analyses

Based on the MWT scale separation results in the previous section, we obtained the average daily KE distribution from August 25 to August 30 by multi-scale energy analysis. Figure 5 shows the variation of daily average KE in the warming-scale window. On August 25, the typhoon Bolaven has not passed through the Yellow Sea region, and the KE of the area along the Mokpo coast is near zero. On August 27, Bolaven began to affect the Mokpo sea area, where the KE increased slightly; On August 28, the typhoon passed through the Mokpo sea area. At this time, the KE increased sharply and reached its peak. It is worth noting that the KE maximum area locates Mokpo SCP where the abnormal warming happens. After that, the KE decreased since Bolaven has landed.

Distribution of the daily KE in the Mokpo sea area in the high-frequency tide-scale window is given by Figure 6. Compared to the other two windows, the high frequency tide-scale window stores most of the KE (the magnitude of this window is greater than the other two). On the 28th, during the passage of typhoon, the KE of the Mokpo area was significantly reduced, while the KE of the warming-scale window increased rapidly (see Figure 5); on the 29th, the KE remained weak; On August 30, the KE rebounded as the typhoon moved away.

In order to further understand the KE changes in these two scales in the Mokpo sea area, Figure 7 shows the time series of the KE of the warming-scale window and the high-frequency tide-scale window. From this we can see that before the passage of Bolaven, the KE of the high-frequency tide-scale window is far greater than the KE of the warming-scale window. However, during the passage of the typhoon through the Mokpo area, the KE of the warming-scale window is rapidly enhanced (K^2). On the 28th, it was even higher than KE in the high-frequency tide-scale scale (K^2).

Next, we pay attention to the changes in the APE of the Mokpo sea area during the passage of the typhoon. Figure 8 shows the time series of the daily APE of Mokpo sea area during the typhoon. It can be seen that the APE in the warming-scale window is always higher than the APE in the high-frequency tide-scale window, and there is no obvious increase during the passage of the typhoon in the Mokpo sea area. It should be noted that the magnitude of the APE is much smaller than the KE. Specifically, in the warming-scale window and the high-frequency tide-scale window, the APE is one order of magnitude smaller

than that of KE. So we focus on the KE change and its underlying dynamic process.

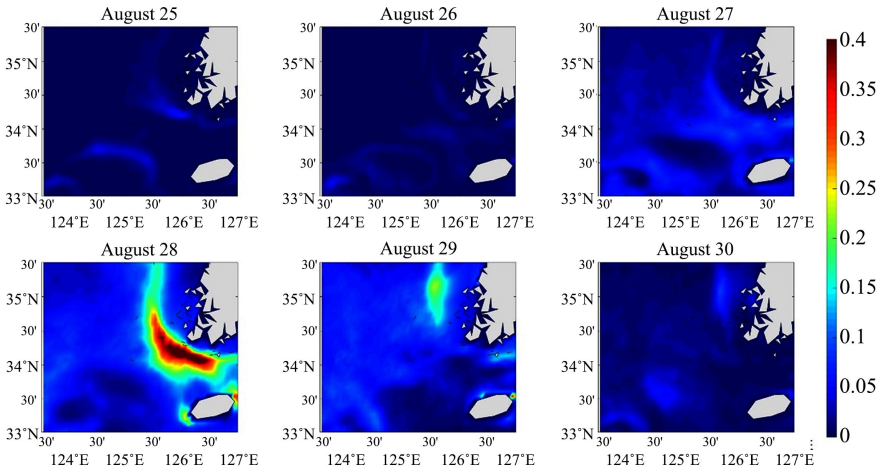

Figure 5. Distribution of daily KE in warming-scale window (K^1) during the passage of Bolaven (unit: J·m^{-3}).

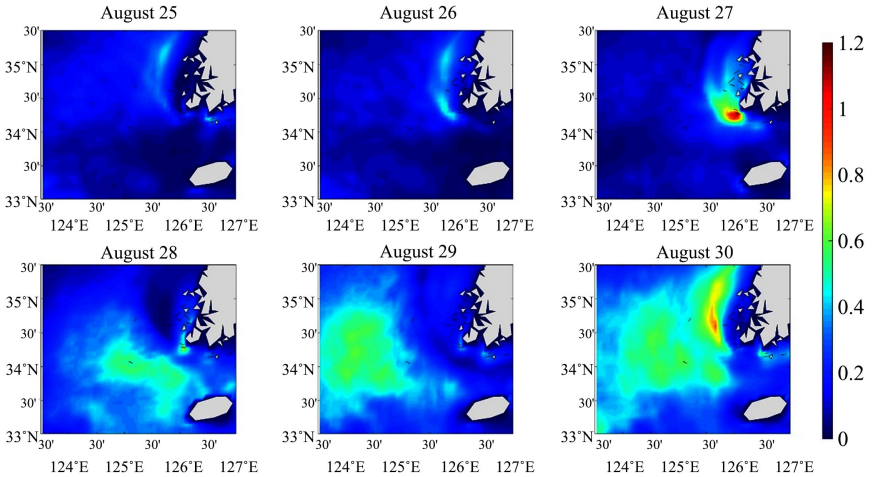

Figure 6. Distribution of daily KE in the high frequency tide-scale window (K^2) during the passage of Bolaven (unit: J·m^{-3}).

Figure 7. Time series of KE of the Mokpo sea area in the warming-scale window (K^1) and high frequency tide-scale window (K^2).

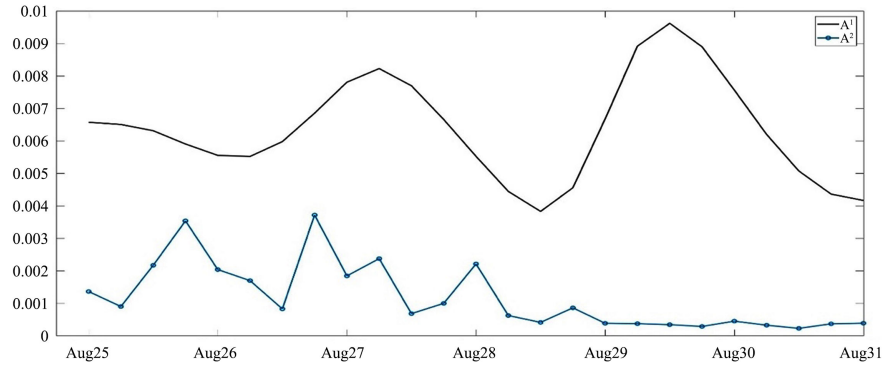

Figure 8. Time series of APE of the Mokpo sea area in the warming-scale window (K^1) and high frequency tide-scale window (K^2).

Generally, energy variability in an ocean domain are mainly influenced by internal ocean process such as baroclinic and barotropic instabilities, or by external atmospheric forcing such as wind stress. In the following we will examine the contribution of internal ocean process and the wind stress work on the KE increase in the warming-scale window.

5.2.1. KE Transfer

We now look at the KE transfer related to the warming-scale window, e.g., $\Gamma_K^{0\to 1}$ and $\Gamma_K^{2\to 1}$. The superscripts $0\to 1$ and $2\to 1$ are used to indicated the transfer from window 0 (large-scale window) to window 1 (warming-scale window) and window 2 (high frequency tide-scale window) to window 1, respectively. It has rigorously established that the transfers correspond precisely to the two important processs in the geophysical fluid dynamic, the barotropic instability (Liang & Robbison, 2007). If we consider the window 0 and 1, the $\Gamma_K^{0\to 1} > 0$ means that warming-scale window receives KE from the large-scale window, thus the system is in the process of barotropic instability.

Figure 9 shows the daily average distribution of KE transfer at the sea level of 2 m, from August 25th to 30th. It can be seen that until August 27, the weak KE transfer appeared in the area along the Mokpo sea area, and there was a negative distribution in northern Mokpo sea area and a positive distribution in southern Mokpo sea area. On the 28th, the typhoon passed through the Mokpo sea area, the KE transfer from large-scale window to the warming-scale window shows strong negative values ($\Gamma_K^{0\to 1} < 0$), which means that the process has the inverse scale KE transfer, that is, the warming-scale window transfers KE to the large-scale window. This result also indicates that the flow field changes have feedback on the low-frequency flow from the large-scale window. As for the 29th, the negative value of the southern Mokpo sea area almost disappears, showing a positive value, which means that the KE of the Mokpo sea area in the warming-scale window is mainly from large-scale window, which indicates the process of barotropic instability; on the 30th, as the typhoon leaves, the transfer of KE in the Mokpo sea area basically disappears.

Compared to large-scale window, the KE transfer of the high-frequency tide-scale window to the warming-scale window $\Gamma_K^{2\to1}$ is stronger. From Figure 10, we can see that before the Bolaven (August 25-27), the KE transfer in the Mokpo sea area are basic positive, which means amounts of KE from the high frequency tide-scale window transfer to the warming-scale window, that is, the inverse scale KE transfer; on the 28th, when the typhoon passes through the Mokpo area, the region exhibits a large range of negative values, indicating that the KE transfer from the warming-scale window to tide-scale window during this period. On the 29th, the negative value of KE transfer in this region reached the peak. On the 30th, as the typhoon moved away, the KE of the region recovered to the condition before the passing of Bolaven, that is, the KE transferred from the high-frequency tide-scale window to the warming- scale window.

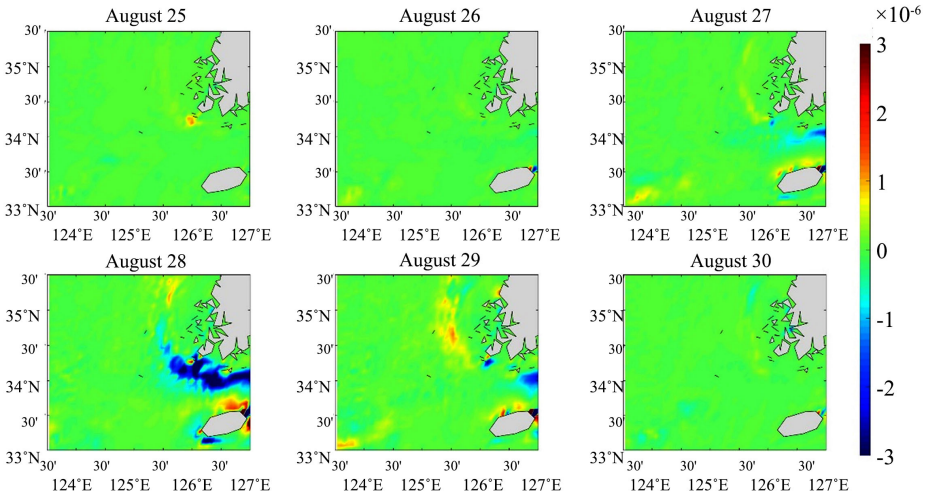

Figure 9. Distribution of daily KE transfer $\Gamma_K^{0\to1}$ (from large-scale window to warming-scale window) in the sea level of 2 m (unit: W·m^{-3}).

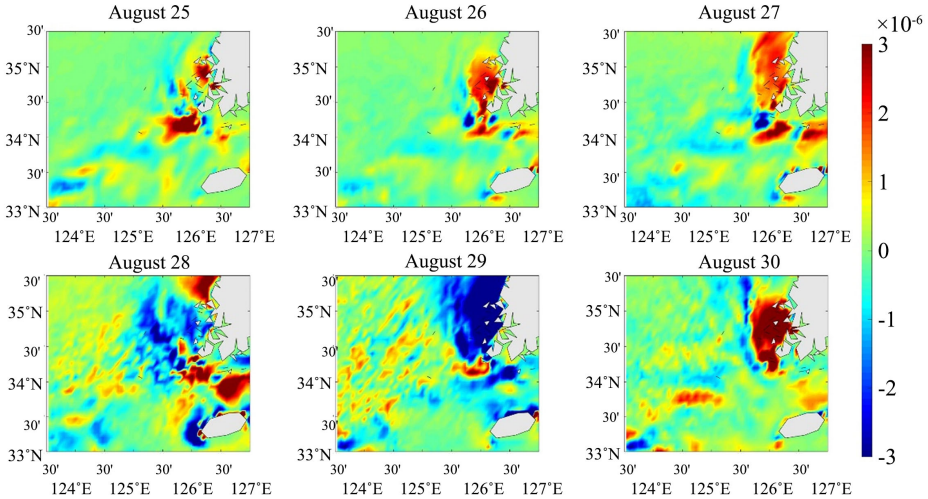

Figure 10. Distribution of daily KE transfer $\Gamma_K^{2\to1}$ (from high frequency tide-scale window to warming-scale window) in the sea level of 2 m (unit: W·m^{-3}).

To sum up, the KE changes in the Mokpo sea area can be divided into two stages, which occur during the passage of typhoon and during the absence of typhoons (i.e., before and after the typhoon passing). Before and after the typhoon passing, there is a strong KE transfer from the tide-scale window to the warming-scale window, that is, the inverse scale KE transfer, while the contribution of KE transfer from large-scale to warming-scale window can be ignored.

During the passage of the typhoon, the KE of the Mokpo region is mainly represented by the transfer of the warming-scale window to the high-frequency tide-scale window. In this case, the KE in the warming-scale window is reduced. On the contrary, there is the relatively weak KE transfer from the large-scale to the warming -scale window. However, Figure 7 tells us that the KE in the warming-scale window experiences a significant increase during the typhoon passage. Therefore, in addition to the process of KE transfer, there must be other processes that contribute to the increase of the KE in the warming-scale window, such as process of the KE flux convergence ($-\nabla\cdot Q_K^1$).

5.2.2. KE Transport

Figure 11 shows the spatial distribution of the KE transport (or KE flux convergence, $-\nabla\cdot Q_K^1$) in the warming-scale window. It can be seen that before the typhoon (August 26-27), the KE transport in the Mokpo sea area is negative and weak; on the 28th, there is a strong negative value area in the southern part of the Mokpo sea area, indicating the appearance of KE flux divergence. On the 29th, the entire Mokpo sea area showed positive values, which represented that the KE flux appeared convergent here; on the 30th, the KE transport returned to the negative distribution before the typhoon passing.

In order to understand the contribution of KE transfer and transport to the KE increase in the warming-scale window, Figure 12 shows the time series of KE transport ($-\nabla\cdot Q_{Kh}^1$, $-\nabla\cdot Q_{Kz}^1$) and transfer ($\Gamma_K^{2\to 1}$, $\Gamma_K^{0\to 1}$) in this scale in the Mokpo sea area. Besides, the conversion between APE and KE (see Section 2 for details) is also given here. In Figure 12, we can see that before the typhoon passed through the Mokpo sea area (August 25-27), the KE was transferred from the high-frequency tide-scale window to the warming-scale window ($\Gamma_K^{2\to 1} > 0$), and the other items changed little. During the passage of typhoon, the KE experienced the inverse scale transfer, that is, from the warming-scale window to the high-frequency tide-scale window subspace ($\Gamma_K^{2\to 1} < 0$). At this time, the horizontal KE flux convergence ($-\nabla\cdot Q_{Kh}^1$) and vertical KE flux convergence ($-\nabla\cdot Q_{Kz}^1$) in the warming-scale window are both positive and strong, which means that the KE transport plays an important role in increasing the KE in the warming-scale window. In addition, the large-scale window also transfers KE to the warming-scale window, which indicates that the barotropic instability process also has a contribution to the increase of KE during this period. After the typhoon, the KE returned to transfer from the tide-scale window to the warming-scale window. The contribution of the buoyancy conversion term throughout the process can be approximately ignored.

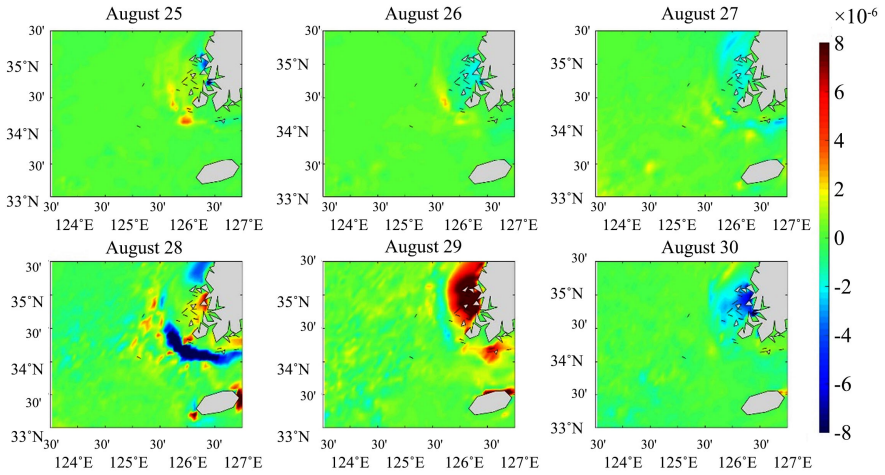

Figure 11. Distribution of KE flux convergence in the warming-scale window ($-\nabla \cdot Q_K^1$). Unit is W·m^{-3}.

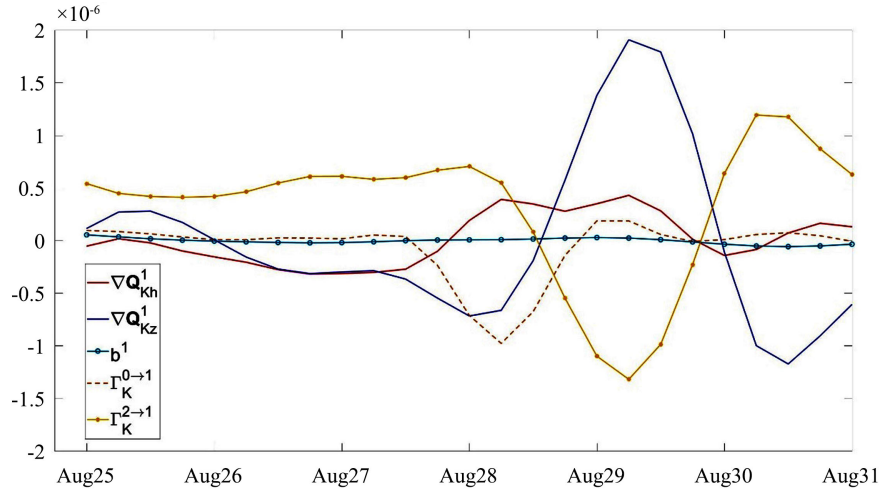

Figure12. Ries of KE flux convergence ($-\nabla \cdot Q_{Kz}^1$, $-\nabla \cdot Q_{Kh}^1$), KE transfer ($\Gamma_K^{2\to 1}$, $\Gamma_K^{0\to 1}$) and buoyance conversion (b^1) in the warming-scale window.

In general, during the passage of Bolaven, the KE rise in the warming-scale window is mainly for KE transport (including vertical and horizontal transport), and the barotropic instability process also plays a role.

5.2.3. Wind Stress Work

The contribution of wind stress work to the KE change during the passage of Bolaven is also explored in this study. Within the MWT-based decomposition results, we can obtain the rate of the wind stress work (F_W^1). Previous studies indicate that wind work to geostrophic currents does not have a large influence on the general circulation, so we choose the geostrophic current for calculation. Following Renault (2017), the F_W^1 is given by:

$$F_W^1 = \frac{1}{\rho_0} \hat{v}_g^{\sim 1} \cdot \hat{\tau}^{\sim 1} \tag{5}$$

where $\hat{v}_g^{\sim 1}$ is the surface geostrophic currents in the warming-scale window and $\hat{\tau}^{\sim 1}$ is the surface wind stress vector in the warming-scale window.

To illustrate the contribution of the wind stress work in the warming-scale window, we plot in Figure 13 the time series of F_W^1 in the Mokpo sea area. One can clearly see that energy input by wind stress (red dashed line in Figure 130s reached peak on August 28, sharing the same trend with KE in warming-scale window (Figure 7). we have already found out that KE flux convergence plays a vital role in the KE rise, so the time series of the KE flux convergence are also plotted in Figure 13 compare with the wind stress work (F_W^1). Figure 13 shows that during the passage of Bolaven, the wind stress energy injection in the warming-scale window is the primary cause of the KE rise, and the KE flux convergence is second.

6. Conclusion

Previous studies have shown that typhoons often cause SST drop. However, this paper pays attention to the abnormal increase of SST induced by Typhoon Bolaven, and studies the related dynamic process of oceanic response in the region where abnormal warming occurs.

As the typhoon Bolaven (2012) passes in August 2012, a warming event occurs in the Yellow Sea outside Mokpo, South Korea. Based on the observation data and high-resolution model ECOM-si output, this study applies a recently developed analysis tool named MWT and the MWT-based localized MS-EVA, to diagnose of the oceanic response to Typhoon Bolaven.

We firstly reconstruct the relative fields onto three scale windows: large-scale, abnormal warming-scale, and high frequency tide-scale windows, and then examine the dynamic process of each window and interaction between different windows. The results show that the KE in the abnormal warming-scale window of the Mokpo area is obviously enhanced during the passage of Bolaven, while the APE changes weakly and is one order of magnitude smaller than the KE.

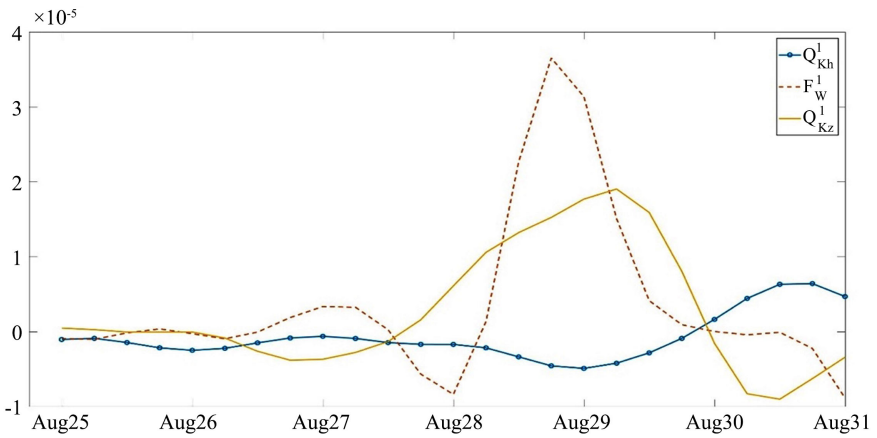

Figure 13. Time series of wind stress work (F_W^1) and vertically integrated KE flux convergence ($-\nabla \cdot Q_{Kh}^1$, $-\nabla \cdot Q_{Kz}^1$) in the warming-scale window. Unit is m^3/s^3.

The results of the energy diagnosis show that during the passage of typhoon, the large-scale window in the Mokpo area experiences barotropic instabilities, accompanied by the KE transfer from the large-scale window to the warming-scale window, which contributes to the increase of the KE in the warming-scale window. At the same time, there is a strong KE transfer from the warming-scale window to the high-frequency tide-scale window, which is not beneficial to the KE increase in the warming scale. Therefore, the process of KE transfer is not the main reason for the increase of KE.

Further studies have found that the increase of KE in the warming-scale window of Mokpo sea area is actually derived from the process of KE transport and wind stress work. The KE transport in the warming-scale window of the Mokpo sea area is significantly enhanced during the passage of the typhoon. In addition, the wind stress work plays the most important role in the KE increase in the warming-scale window. Generally, the contribution of wind stress is the largest, and the KE flux convergence is second.

Conflicts of Interest

The authors declare no conflicts of interest regarding the publication of this paper.

References

Chang, G. C., Dickey, T. D., & Williams III, A. J. (2001). Sediment Resuspension over a Continental Shelf during Hurricanes Edouard and Hortense. *Journal of Geophysical Research Oceans, 106,* 9517-9531. https://doi.org/10.1029/2000JC900032

Chang, S. K., Lim, H.-S., Jeong, J. Y., Shim, J.-S., Moon, I.-J., Oh, Y. J., & You, H. Y. (2014). Responses of Coastal Waters in the Yellow Sea to Typhoon Bolaven (2012). *Journal of Coastal Research, 70,* 278-283. https://doi.org/10.2112/SI70-047.1

Chang, Y.-C., Tseng, R.-S., & Centurioni, L. R. (2010). Typhoon-Induced Strong Surface Flows in the Taiwan Strait and Pacific. *Journal of Oceanography, 66,* 175-182. https://doi.org/10.1007/s10872-010-0015-y

Chen, D., Lei, X., Wang, W., Wang, G., Han, G., & Zhou, L. (2013). Upper Ocean Response and Feedback Mechanisms to Typhoon. *Advances in Earth Science, 28,* 1077-1086. (In Chinese)

Cheng, X., Li, L., Du, Y., Wang, J., & Huang, R. X. (2013). Mass-Induced Sea Level Change in the Northwestern North Pacific and Its Contribution to Total Sea Level Change. *Geophysical Research Letters, 40,* 3975-3980. https://doi.org/10.1002/grl.50748

D'Asaro, E. A., Black, P. G., Centurioni, L. R., Chang, Y.-T., Chen, S. S., Foster, R. C., Graber, H. C., Harr, P., Hormann, V., Lien, R.-C., Lin, I.-I., Sanford, T. B., Tang, T.-Y., & Wu, C.-C. (2013). Impact of Typhoons on the Ocean in the Pacific. *Bulletin of the American Meteorological Society 95,* 1405-1418. https://doi.org/10.1175/BAMS-D-12-00104.1

Han, G., Ma, Z., Chen, N., Chen, N., Yang, J., & Chen, D. (2017). Hurricane Isaac Storm Surges off Florida Observed by Jason-1 and Jason-2 Satellite Altimeters. *Remote Sensing of Environment, 198,* 244-253. https://doi.org/10.1016/j.rse.2017.06.005

He, H. L., Wu, Q., Chen, D., Sun, J., Liang, C., Jin, W. et al. (2018). Effects of Surface Waves and Sea Spray on Air-Sea Fluxes during the Passage of Typhoon Hagupit. *Acta*

Oceanologica Sinica, 37, 1-7. https://doi.org/10.1007/s13131-018-1208-2

Huang, M., Liang, X. S., Wu, H., & Wang, Y. (2017). Different Generating Mechanisms for the Summer Surface Cold Patches in the Yellow Sea. *Atmosphere-Ocean, 56,* 199-211. https://doi.org/10.1080/07055900.2017.1371580

Huang, W., Mukherjee, D., & Chen, S. (2011). Assessment of Hurricane Ivan Impact on Chlorophyll-a in Pensacola Bay by MODIS 250 m Remote Sensing. *Marine Pollution Bulletin, 62,* 490-498. https://doi.org/10.1016/j.marpolbul.2010.12.010

Lee, J. H., Moon, I.-J., Moon, J.-H., Kim, S.-H., Jeong, Y. Y., & Koo, J.-H. (2017). Impact of Typhoons on the Changjiang Plume Extension in the Yellow and East China Seas: Impact of Typhoons on Changjiang Plume. *Journal of Geophysical Research: Oceans, 122,* 4962-4973. https://doi.org/10.1002/2017JC012754

Li, L., & Xu, J. (1994). Notes on Response of Coastal Waters to Typhoon Passage I. Response of Daya Bay Hydrological Conditions to Typhoons No. 8708 and No. 8710. *Journal of Oceanography in Taiwan Strait, 13,* 213-218. (In Chinese)

Li, Y., Wang, A., Qiao, L., Fang, J., & Chen, J. (2012). The Impact of Typhoon Morakot on the Modern Sedimentary Environment of the Mud Deposition Center off the Zhejiang-Fujian Coast, China. *Continental Shelf Research, 37,* 92-100. https://doi.org/10.1016/j.csr.2012.02.020

Liang, X. S. (2016). Canonical Transfer and Multiscale Energetics for Primitive and Quasi-Geostrophic Atmospheres. *Journal of the Atmospheric Sciences, 73,* 4439-4468. https://doi.org/10.1175/JAS-D-16-0131.1

Liang, X. S., & Robinson, A. R. (2007). Localized Multi-Scale Energy and Vorticity Analysis: II. Finite-Amplitude Instability Theory and Validation. *Dynamics of Atmospheres and Oceans, 44,* 51-76. https://doi.org/10.1016/j.dynatmoce.2007.04.001

Lin, I.-I., Wu, C.-C., Pun, I.-F., & Ko, D.-S. (2008). Upper-Ocean Thermal Structure and the Western North Pacific Category 5 Typhoons. Part I: Ocean Features and the Category 5 Typhoons' Intensification. *Monthly Weather Review, 137,* 3744-3757. https://doi.org/10.1175/2009MWR2713.1

Liu, Z., Xu, J., Sun, C., & Wu, X. (2014). An Upper Ocean Response to Typhoon Bolaven (2012) Analyzed with Argo Profiling Floats. *Acta Oceanologica Sinica, 33,* 90-101. https://doi.org/10.1007/s13131-014-0558-7

Moon, I.-J., & Kwon, S. J. (2012). Impact of Upper-Ocean Thermal Structure on the Intensity of Korean Peninsular Landfall Typhoons. *Progress in Oceanography, 105,* 61-66. https://doi.org/10.1016/j.pocean.2012.04.008

Price, J. F. (1981). Upper Ocean Response to a Hurricane. *Journal of Physical Oceanography, 11,* 153-175. https://doi.org/10.1175/1520-0485(1981)011<0153:UORTAH>2.0.CO;2

Renault, C. (2017). Relative Equilibria with Holes for the Surface Quasi-Geostrophic Equations. *Journal of Differential Equations, 263,* 567-614. https://doi.org/10.1016/j.jde.2017.02.050

Wang, L., & Liang, X. S. (2017). A Diagnosis of Some Dynamical Processes Underlying a Higher-Latitude Typhoon Using the Multiscale Window Transform. *Atmosphere, 8,* 118. https://doi.org/10.3390/atmos8070118

Wu, H., Shen, J., Zhu, J., Zhang, J., & Li, L. (2014). Characteristics of the Changjiang Plume and Its Extension along the Jiangsu Coast. *Continental Shelf Research, 76,* 108-123. https://doi.org/10.1016/j.csr.2014.01.007

Wu, H., Zhu, J., Shen, J., & Wang, H. (2011). Tidal Modulation on the Changjiang River Plume in Summer. *Journal of Geophysical Research: Atmospheres, 116,* 192-197.

https://doi.org/10.1029/2011JC007209

Xie, L. L., He, C.-F., Li, M.-M., Tian, J. J., & Jing, Z. Y. (2017). Response of Sea Surface Temperature to Typhoon Passages over the Upwelling Zone East of Hainan Island. *Advances in Marine Science, 35,* 8-19. (In Chinese)

Yang, G.-B., Lü, L.-G., Zhuang, Z.-P., Xiong, X.-J., Wang, G.-S., Guo, Y.-L., Yu, L., & Ma, D.-J. (2017). Cruise Observation of Shallow Water Response to Typhoon Damrey 2012 in the Yellow Sea. *Continental Shelf Research, 148,* 1-8. https://doi.org/10.1016/j.csr.2017.09.006

Zhang, H., Chen, D., Zhou, L., Liu, X., Ding, T., & Zhou, B. (2016). Upper Ocean Response to Typhoon Kalmaegi (2014): Upper Ocean Response to Kalmaegi (2014). *Journal of Geophysical Research: Oceans, 121,* 6520-6535. https://doi.org/10.1002/2016JC012064